# ALD-passivated silicon nanowires for broadband absorption applications

Cite as: AIP Advances 11, 065101 (2021); https://doi.org/10.1063/5.0054104 Submitted: 14 April 2021 • Accepted: 11 May 2021 • Published Online: 01 June 2021

Felix Kimeu, Sacharia Albin, Kyo Song, et al.









## ARTICLES YOU MAY BE INTERESTED IN

Conformality in atomic layer deposition: Current status overview of analysis and modelling Applied Physics Reviews 6, 021302 (2019); https://doi.org/10.1063/1.5060967

Origins of the enhanced broadband absorption in black silicon

Journal of Applied Physics 129, 163103 (2021); https://doi.org/10.1063/5.0047153

Understanding chemical and physical mechanisms in atomic layer deposition
The Journal of Chemical Physics 152, 040902 (2020); https://doi.org/10.1063/1.5133390





# ALD-passivated silicon nanowires for broadband absorption applications

Cite as: AIP Advances 11, 065101 (2021); doi: 10.1063/5.0054104

Submitted: 14 April 2021 • Accepted: 11 May 2021 •

Published Online: 1 June 2021







Felix Kimeu, Sacharia Albin, Kyo Song, and Kevin C. Santiago 10

# **AFFILIATIONS**

Electronics Engineering Department, Norfolk State University, Norfolk, Virginia 23462, USA

a) Author to whom correspondence should be addressed: ksantial@nsu.edu and kcsantiago@nsu.edu

## **ABSTRACT**

Silicon photonics enables the fabrication of optical devices with standard semiconductor processing technology. With high transparency and modal confinement, Si has matured into a well-established infrared optical material. Nanostructured silicon has been studied extensively due to its optical properties, especially silicon nanowires due to the myriad of available fabrication techniques, the broad range of physical dimensions, and the resulting optical characteristics. In this study, we fabricate silicon nanowires using a wet chemical process and modify their absorptive properties via atomic layer deposition passivation. The passivated nanowires absorb 95% of light from the visible to infrared, with a minimal angular dependence, making them excellent candidates for broadband absorber applications.

© 2021 Author(s). All article content, except where otherwise noted, is licensed under a Creative Commons Attribution (CC BY) license (http://creativecommons.org/licenses/by/4.0/). https://doi.org/10.1063/5.0054104

## INTRODUCTION

Silicon nanowires (SiNWs) have attracted much interest over recent years due to their remarkable material properties. With suitable fabrication parameters, SiNWs may have a high surface area, low electrical resistance, and low optical reflectivity. 1-4 Several methods have been developed to fabricate SiNWs, such as liquid-vapor-solid growth, reactive-ion etching, and Metal-Assisted Chemical Etching (MACE).<sup>3-6</sup> MACE processing is a relatively simple and low-cost technique, which can be modified to control the morphology of SiNWs. The etch rate depends on several parameters such as reaction time, temperature, chemical concentration, and ambient environment. Silicon is a high index optical material—when the diameter of SiNWs is near that of the wavelength of incident light, strong resonant field enhancement and absorption enable many applications. The subsequent material properties make it possible to enhance optoelectronics, thermoelectrics, biomedical devices, and even energy storage devices.7

Many studies focused on optimizing SiNWs to fine tune the optical properties. 11-16 Nonlinear responses and several other optical phenomena have been observed in SiNWs when in combination with complimentary material systems and rare-earth elements. Previous reports suggest that bunched SiNWs (which are usually wet-processed) are efficient at absorbing visible light but less efficient in longer wavelengths. Multiple resonant reflections

occur between bunched nanowire tips, where the distance between adjacent wires is comparable to an integer multiple of wavelength of light, suitable for destructive interference. Alternatively, highly ordered SiNW efficiency quenches light in the infrared regime but requires more precise fabrication strategies (photolithography and etching). At longer wavelengths, the distance required between SiNWs needed for destructive interference is larger. Therefore, the wire-to-wire distance must be further and tightly controlled. Ultimately, the optical absorption profile of SiNWs is determined by the morphology and spatial distribution, as well as the incident light parameters.

A study by Gaboriau *et al.* used Atomic Layer Deposition (ALD)-coated SiNWs for energy storage applications. <sup>10</sup> In this study, a thin layer of alumina was deposited on SiNWs via ALD and characterized in terms of energy storage capability. Surprisingly, the use of ALD-coated SiNWs has never been applied to broadband optical absorbers. Although the application is different, this approach provides an insulating layer that passivates sharp edges of the SiNWs. Moreover, ALD may be used to modify the effective wire-to-wire distance between SiNWs, causing a shift in the resonant interference conditions, as well as the angular dependence of reflectance due to refraction at multiple surfaces. In this study, we fabricate SiNWs using the MACE technique, passivate the wires using a thin oxide layer, and investigate the broadband absorption capabilities of the composite SiNW-oxide matrix.

#### **EXPERIMENTAL DETAILS**

Boron-doped (100) silicon wafers were used as substrates. Each wafer was cut into  $2\,\mathrm{cm}^2$  samples using a *Fusion* M2 cutting/engraving laser. The substrate preparation process included various steps: first, the samples were sonicated in acetone and isopropanol for 5 min each at  $20\,^\circ\mathrm{C}$ . Then, the cleaned samples were dipped in piranha solution (97%  $\mathrm{H_2SO_4/30W\ H_2O_2}$ ) at a ratio of 3:1 for 10 min, removing the organic matter and hydroxylates. This step was followed by rinsing with DI water. A buffered oxide etch followed, with the samples being placed in 5% aqueous HF for 3 min to remove any underlying SiO<sub>2</sub>.

After cleaning, SiNWs of various morphologies were fabricated using the two-step MACE process.<sup>17</sup> The samples were placed in an Ag-coating solution containing 4.8M HF and 0.02M silver nitrate (AgNO<sub>3</sub>), stirring them slowly for 1 min. Increasing the reaction time increases the conformal coverage of the Ag reaction sites on the Si surface, leading to a higher density of SiNWs. For this fabrication process, a 60-s deposition time was used as the control, as it resulted in a vertically aligned uniform SiNW distribution. After the first step, the samples were rinsed with DI water to remove excess Ag<sup>+</sup> ions. The samples were then dipped in the etching solution composed of 4.8M HF and 0.15M H<sub>2</sub>O<sub>2</sub> for different etching durations, ranging from 10 to 60 min, at room temperature. At the end of each etching period, the samples were rinsed repeatedly with DI water and then dipped in nitric acid for 10 min to remove any residual dendrites. As a final step, the samples were dipped in 5% HF again to remove the oxide layer, and then, they were rinsed with DI water. The samples were then dried using nitrogen gas and taken for further processing and characterization.

A passivation layer of  $HfO_2$  was deposited on the various SiNW samples with different etch times. The deposition system was *Cambridge Nanotech Savannah S100*.  $HfO_2$  was the most readily available precursor in our lab and chosen due to its high transparency and index over a broad spectral range. The use of other ALD-deposited materials will be the basis of future studies. The chemical precursors were tetrakis(diethylamido)hafnium(IV) and water, which were pulsed sequentially for 0.4 and 0.015 s, respectively, with 10 s intervals between pulses. Each cycle deposited  $\sim 1.6$  Å of oxide. Deposition of 150 cycles at a temperature of  $200\,^{\circ}$ C, with  $N_2$  used as a carrier gas at 20 SCCM, was used as a control. This resulted in a 25 nm-thick layer of  $HfO_2$ . A silicon blank was placed in the ALD chamber and taken for reference measurements.

Spectroscopic scans of the SiNWs, HfO<sub>2</sub>, and ALD-passivated SiNWs were carried out using a VASE HS 190 ellipsometer. The scans ranged from 400 to 800 nm, in 10 nm steps, at scan angles of 60°, 65°, and 70°. This resulted in over 300 data points per sample to be fitted via modeling. The models were developed using the WVASE32 software. The optical properties of the constituent materials were measured and modeled prior to being imported in the combined material system. The SiNW samples and ALD-passivated samples were modeled as stratified sublayers, each composed of different proportions of materials [Si and void (air) for SiNWs and Si and HfO<sub>2</sub> for the passivated wires, assuming that the ALD process completely filled gaps between wires]. The Bruggeman Effective Medium Approximation (EMA) was used to describe the optical response of the mixture of materials in each layer. <sup>13,18</sup> In these optical models, the unknown parameters included roughness and

the proportions of the constituent materials in each sublayer. The unknown parameters are varied iteratively to achieve the best fit between the experimental data and the simulated data. The process is followed for each sublayer while observing the response of the RMSE.

The polarized reflectance was also measured using VASE HS 190. A silicon blank was used as a reference to establish a baseline intensity for each wavelength, polarization, and angle. The scans ranged from 400 to 800 nm, in 10 nm steps, with scan angles ranging from  $65^{\circ}$  to  $85^{\circ}$  in  $5^{\circ}$  steps.

## **RESULTS AND DISCUSSION**

In Table I, we present the resulting SiNW length vs the submersion time in the MACE solution. The data shown in this study are from samples with a 30-min etch time. Samples with a 30-min etch time had the most consistent vertically aligned and densely packed wires across the sample surface, which resulted in the lowest reflectance values measured across all samples. The bunching of SiNWs beyond the 30-min etch time is due to the electrostatic interactions that take place when the nanowires reach an aspect ratio of ~16:1. At these high ratios, the stiffness decreases, and they are more susceptible to falling over and/or stiction with neighboring wires. Samples with lower etch times suffered from large gap spaces between wires or pockets on the sample surface where the etching was inconsistent. The samples with an etch time longer than 30 min resulted in SiNWs that were not vertically aligned and bunched near wire tips. Bunching increased the reflectance of the samples due to the light's inability to scatter effectively between NWs, which is the primary method of extinction of light at the air/SiNW interface. The wire length ultimately depends on the etching time and concentration of silver nitrate (AgNO<sub>3</sub>) during MACE. If different dimensions are desired, changing the molar ratio of silver nitrate would be the most convenient method.

Figure 1 shows a cross-sectional SEM image of a SiNW sample (a) and the associated model used to describe the spectroscopic ellipsometry data (b). A 1-µm scale bar is shown for reference. The SiNWs were modeled as four independent sublayers. The silicon:air ratio varies in each sublayer, with the root of the SiNWs being modeled as an interfacial mixing layer. The B-EMA was employed to fit the uniform SiNW layer. The top layer was modeled as surface roughness, which sets the ratio between silicon and air at 50:50. Although some SiO<sub>2</sub> may be present in the samples, its optical response is near identical to that of air; therefore, it is omitted in the models used for this study. <sup>19</sup> Several independent sublayers were used in the model; the cut-off wavelength used for the fitting of the model was chosen intuitively by selecting sufficiently large upper

TABLE I. Etch time vs SiNW length.

Etch time (min)	SiNW length (nm)
10	1093.47
20	1427.62
30	1934.13
40	2327.45
50	3234.12

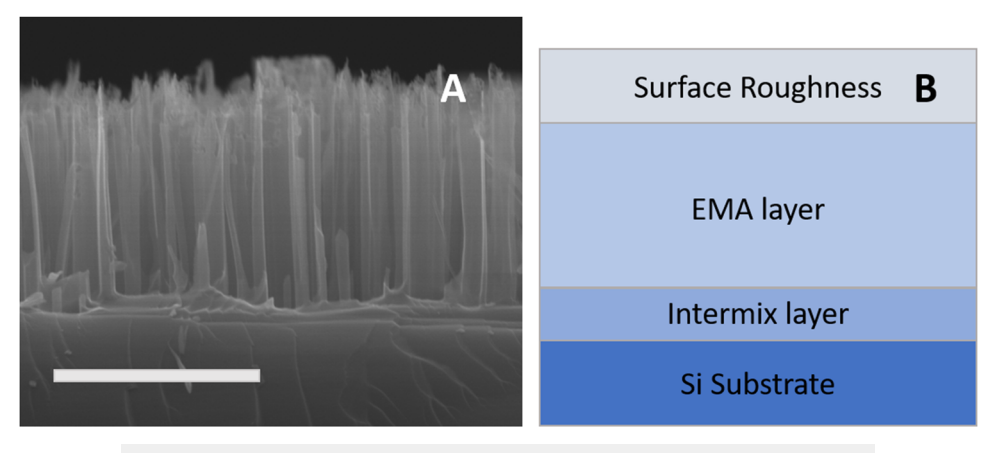


FIG. 1. (a) Cross-sectional SEM image of the SiNWs and (b) corresponding SiNW VASE model.

spectra, then decreasing it in a step-wise manner, and monitoring the RMSE value to determine the fit quality.  $^{13}$ 

Figure 2 shows the optical properties of the constituent materials used in the ALD-passivated SiNWs. The SiNW model is consistent with the schematic in Fig. 1(b). The MSE value for all the SiNW models was near 6.5, with most of the error occurring near the S-polarized near infrared portion of the scan range. The effective index values are well below that of bulk Si, which usually vary from 5.5 to 3.7 depending on the doping concentration and oscillator model used. We attribute the difference to the presence of air between the SiNWs, instead of the bulk crystal, which has a higher optical density than the wire array. The HFO2 oscillator model in the WVASE material library was used to describe ALD-grown oxide. The thickness of HFO2 was verified; for a film thickness of ~25 nm, the MSE value was below 2. The associated optical properties are consistent with those found in the literature for this particular growth method.  $^{21,22}$  There is a significant decrease in the k-values for both SiNWs and

HFO $_2$  beyond 400–450 nm. For the SiNWs, the dispersion model is a combination of the bulk p-type silicon properties and nanowire effects. The Tauc–Lorentz dielectric function was used to model the raw VASE data while using a step function to minimize the MSE value in the longer part of the spectrum. The k-values are consistent with those found elsewhere in the literature. $^{23}$ 

The optical properties of  $HfO_2$  are largely determined by the deposition technique (in this case ALD) and the substrate/film interface properties.  $HfO_2$  deposited by ALD has a large bandgap, ranging from 5.3 to 5.9 eV (depending on the phase) with low optical absorption through the visible and IR, and hence the low k value beyond 450 nm. The k values for both SiNWs and  $HfO_2$  are relatively low from 400 to 800 nm. This would suggest that the primary method extinction is the multiple scattering events that take place when light enters the nanowire matrix, which would result in the eventual absorption at the bulk Si/intermix layer, as bulk Si has a significantly higher k value in the aforementioned scan range.

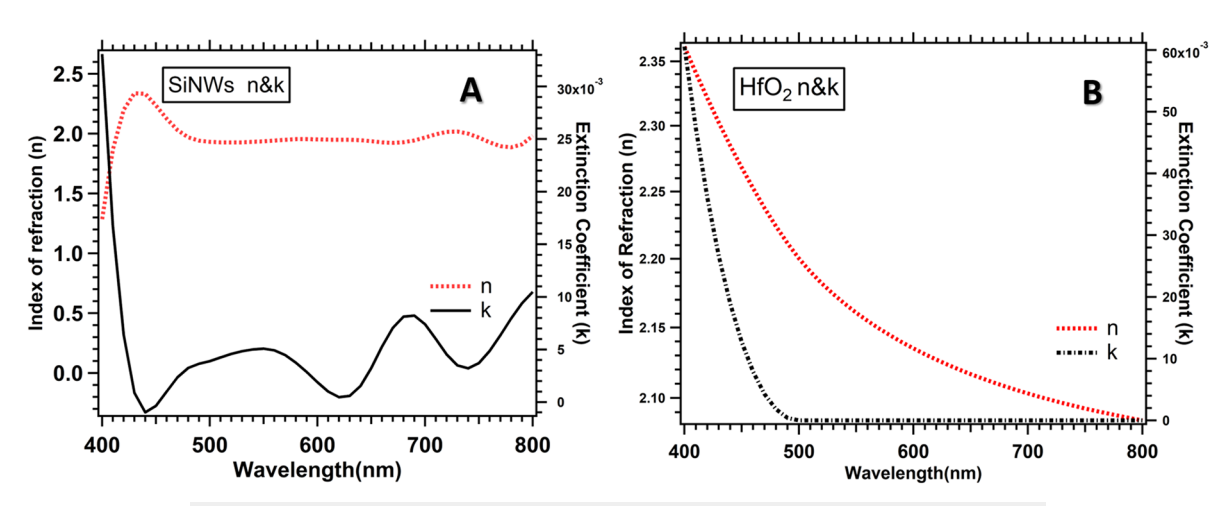


FIG. 2. (a) Fitted n & k values for SiNWs w/30-min etch and (b) fitted n & k values for 25 nm ALD-grown HfO<sub>2</sub>.

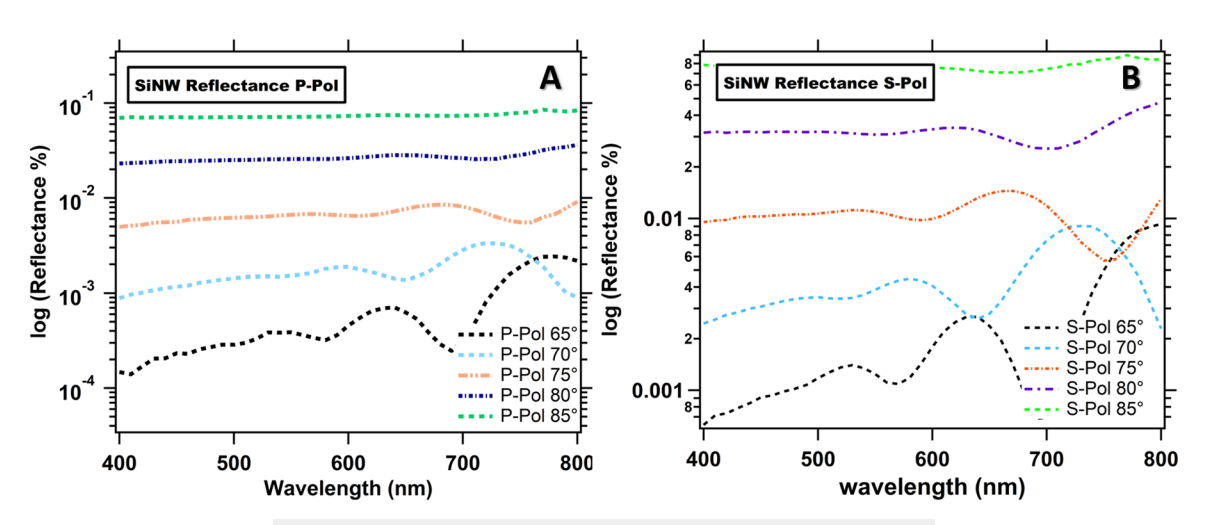


FIG. 3. (a) SiNW P-polarization reflectance and (b) SiNW S-polarization reflectance.

Figure 3 shows the log-scale reflectance of the SiNWs with (a) P-polarized and (b) S-polarized light at various incidence angles. The P-polarized reflectance is near 10<sup>-4</sup> at 65° and increases as a function of wavelength. It also increases as the incidence angle approaches grazing conditions. There is a local minimum that occurs near 700 nm, which corresponds to a local maximum in the effective extinction values for the SiNWs. A gradual increase in reflectance is observed with an increase in the angle, which would suggest that the light effectively backscatters at higher angles of incidence, instead of being trapped within the nanowire matrix. At 85°, the reflectance approaches  $10^{-1}$ , which corresponds to the array absorbing ~94% of light. The S-polarized light follows a similar trend while being nearly an order of magnitude higher in reflectance than that of the P-polarized light at each incidence angle. The downward scattering efficiency of light polarized perpendicular to the plane of incidence may be higher, as the E-field oscillates in the long axis of the wires and has a higher probability to scatter toward the intermix/bulk Si. When the E-field oscillates parallel to the plane of incidence (short axis of the wires), it has less light-matter interaction and therefore a higher probability of backscatter from the NW/air interface.<sup>24</sup>

Figure 4 shows a cross-sectional SEM image of the HFO<sub>2</sub>-coated SiNWs with a 1- $\mu$ m scale bar (a) and the corresponding WVASE model used to fit the spectroscopic data (b). The ALD-deposited oxide completely filled the gap spaces between SiNWs, forming a composite with a relatively uniform interface (some surface roughness is present). One interesting note is that the oxide dramatically increased the mechanical stability of the SiNWs. Standalone SiNWs were easily scratched and/or peeled off the bulk sample surface, so delicate handling was required. The oxide layer serves as a protective coating, in addition to dramatically reducing the reflectance varying as a function of wavelength (see Fig. 5).

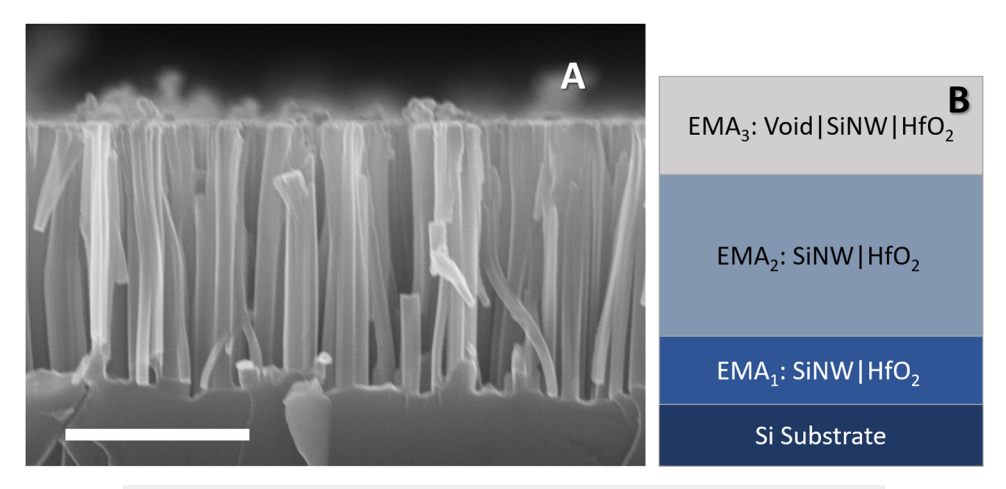


FIG. 4. (a) Cross-sectional SEM image of the HfO<sub>2</sub> coated SiNWs and (b) the EMA VASE model.

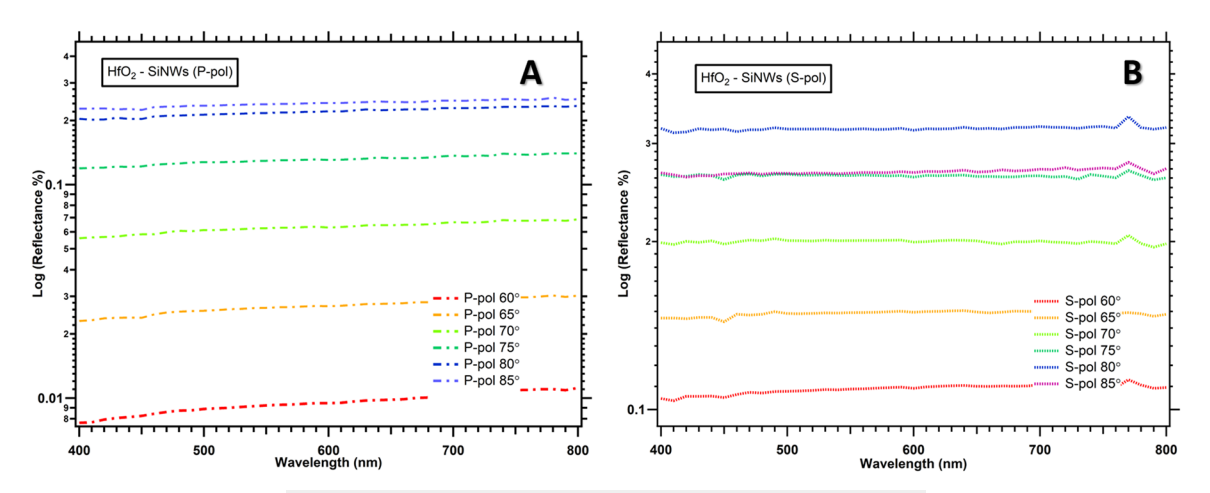


FIG. 5. Hafnium oxide on SiNWs: (a) P-polarized and (b) S-polarized reflectance.

The main drawback to the HFO<sub>2</sub> layer is the increase in reflectance at each angle due to the planar interface at the HFO<sub>2</sub>/air boundary, resulting in Fresnel reflections. <sup>25</sup> For the stand-alone SiNWs, the reflectance (%) was near  $10^{-4}$  at  $65^{\circ}$ ; with the addition of the oxide, this increased to  $\sim 10^{-3}$ . This may be circumvented by slightly reducing the thickness of the deposited oxide layer such that the interface maintains some wire-to-wire separation and allows the light to effectively scatter into the composite matrix. Another way to alleviate this issue would be to deposit an oxide layer with a lower refractive index so that the difference in the index between air and oxide is lower, resulting in reduced back reflections. <sup>26</sup> Investigating other oxide systems will be the basis of future studies.

Although the reflectance increases, the polarization and angular dependence on absorbance is significantly reduced. This may be credited to the fact that the oxide filling between the wires acts as a complimentary optical medium in which the light may refract/scatter into, independent of the orientation of the E-field. Once light has entered the composite, the light is internally reflected instead of propagating back into air. The S- and P-polarized light are now within the same order of magnitude in terms of reflectance, as opposed to the stand-alone SiNWs where the difference between the two polarizations was near 2 orders of magnitude. For both polarizations, the reflectance curves are relatively flat across the entire visible

band (400–800 nm) instead of the heavy dependence on the wavelength. This is likely due to the interface characteristics of the composite. The stand-alone SiNWs create resonances at specific wavelengths due to the diameter of the wires and the wire-to-wire spacing (especially for S-polarized light). When filled with ALD-grown oxide, these resonant fields are no longer able to propagate back into air but are likely refracted back into the composite, especially at higher incidence angles.

In Table II, we compare recent work on nanostructured absorbers with the work presented here. Vantablack continues to be the darkest material ever created, absorbing 99.995% of light across a broad range of wavelengths.<sup>27–29</sup> Carbon nanotube systems are leading in terms of absorption efficiency but are much more expensive and mechanically fragile.<sup>30–33</sup> MACE-processed SiNW absorbers may attenuate up to 99.8% of light while being less costly to produce. The absorption properties may be further engineered by optimizing the fabrication parameters and passivating the system with an ALD-grown layer that provides mechanical stability. SiNW composites may be an alternative for absorber applications that require mechanical resilience or systems that are exposed to corrosive/destructive environments. With careful parameter control and post-fabrication engineering, it may be possible to increase the attenuation beyond 99.8%.

TABLE II. Attenuation comparison of nanowire systems.

Material	Researchers	Attenuation (%)	Reflectance (%)
SiNW arrays	17	99.1	0.9
VANTA-black	18	99.965	0.035
Vertically aligned carbon nanotubes	19	99.995	0.005
SiNW arrays	20	99.8	0.2
ALD-passivated SiNW arrays (this work)	22	99.8	0.2
SiNWs at a wide angle of 60°	14	80-85	15-20

#### CONCLUSION

In conclusion, we fabricated SiNWs using a MACE process and modified their optical properties by atomic layer-deposited oxide passivation. This created an oxide-nanowire matrix that significantly altered the reflectance capability. The stand-alone NWs absorb nearly 99.2% of light at low incidence angles but were largely dependent on polarization and wavelength and also mechanically fragile. The passivated nanowires absorb 95% of light from the visible to near infrared, with a reduced angular dependence and a minimal polarization dependence, while simultaneously enhancing their mechanical strength. With fine tuning of the fabrication parameters (MACE variables and oxide thickness), the reflectance can be significantly reduced, as the main reason for the increase in reflectance was the planar interface of the oxide-nanowire matrix. Owing to their surface-dependent physical, chemical, and optical properties, these absorbers can be used in applications such as catalysis, biosensors, batteries, and solar cells.<sup>34,35</sup> Future work includes optimizing the MACE chemistry to reduce the diameter of the SiNWs and investigating different oxides that would further reduce the Fresnel reflections at the interface.

## **ACKNOWLEDGMENTS**

The authors declare no conflicts of interest.

## **DATA AVAILABILITY**

The data that support the findings of this study are available from the corresponding author upon reasonable request.

## **REFERENCES**

- <sup>1</sup>M. Hasan, M. F. Huq, and Z. H. Mahmood, "A review on electronic and optical properties of silicon nanowire and its different growth techniques," SpringerPlus **2**(1), 151 (2013).
- <sup>2</sup>S. D. Hutagalung, M. M. Fadhali, R. A. Areshi, and F. D. Tan, "Optical and electrical characteristics of silicon nanowires prepared by electroless etching," Nanoscale Res. Lett. 12(1), 425 (2017).
- <sup>3</sup>X. Weng *et al.*, "Review of the preparation and structures of Si nanowires, Ge quantum dots and their composites," Nano **14**(04), 1930004 (2019).
- <sup>4</sup>V. Schmidt, J. V. Wittemann, S. Senz, and U. Gösele, "Silicon nanowires: A review on aspects of their growth and their electrical properties," Adv. Mater. **21**(25-26), 2681–2702 (2009).
- <sup>5</sup>T. Yamaguchi *et al.*, "Morphology dependence of optical reflectance properties for a high-density array of silicon nanowires," Jpn. J. Appl. Phys., Part 1 53(6S), 06JF10 (2014).
- <sup>6</sup>Z. Dong, W. Rong, Y. Zhang, and X. Deng, "Light-assisted MACE method for the control of silicon nanowire morphology," IOP Conf. Ser.: Mater. Sci. Eng. **394**, 032102 (2018).
- <sup>7</sup>G. Brönstrup, N. Jahr, C. Leiterer, A. Csáki, W. Fritzsche, and S. Christiansen, "Optical properties of individual silicon nanowires for photonic devices," ACS Nano 4(12), 7113–7122 (2010).
- <sup>8</sup>A. I. Boukai, Y. Bunimovich, J. Tahir-Kheli, J.-K. Yu, W. A. Goddard III, and J. R. Heath, "Silicon nanowires as efficient thermoelectric materials," Nature 451(7175), 168–171 (2008).
- <sup>9</sup>S. Qi, C. Yi, W. Chen, C.-C. Fong, S.-T. Lee, and M. Yang, "Effects of silicon nanowires on HepG2 cell adhesion and spreading," ChemBioChem 8(10), 1115–1118 (2007).
- <sup>10</sup>D. Gaboriau *et al.*, "Atomic layer deposition alumina-passivated silicon nanowires: Probing the transition from electrochemical double-layer capacitor to electrolytic capacitor," ACS Appl. Mater. Interfaces 9(15), 13761–13769 (2017).

- <sup>11</sup>H. Bao and X. Ruan, "Optical absorption enhancement in disordered vertical silicon nanowire arrays for photovoltaic applications," Opt. Lett. 35(20), 3378 (2010).
- <sup>12</sup>M. M. Adachi, M. P. Anantram, and K. S. Karim, "Optical properties of crystalline-amorphous core-shell silicon nanowires," Nano Lett. 10(10), 4093–4098 (2010).
- <sup>13</sup>B. Fodor, T. Defforge, E. Agócs, M. Fried, G. Gautier, and P. Petrik, "Spectroscopic ellipsometry of columnar porous Si thin films and Si nanowires," Appl. Surf. Sci. 421, 397–404 (2017).
- 14.Y. F. Zhang, L. S. Liao, W. H. Chan, S. T. Lee, R. Sammynaiken, and T. K. Sham, "Electronic structure of silicon nanowires: A photoemission and x-ray absorption study," Phys. Rev. B 61(12), 8298–8305 (2000).
- <sup>15</sup>H. Park *et al.*, "Filter-free image sensor pixels comprising silicon nanowires with selective color absorption," Nano Lett. **14**(4), 1804–1809 (2014).
- <sup>16</sup>M. Hocevar *et al.*, "Growth and optical properties of axial hybrid III–V/silicon nanowires," Nat. Commun. 3(1), 1266 (2012).
- <sup>17</sup>L. U. Vinzons, L. Shu, S. Yip, C.-Y. Wong, L. L. H. Chan, and J. C. Ho, "Unraveling the morphological evolution and etching kinetics of porous silicon nanowires during metal-assisted chemical etching," Nanoscale Res. Lett. **12**, 385 (2017)
- <sup>18</sup>M. Khardani, M. Bouaïcha, and B. Bessaïs, "Bruggeman effective medium approach for modelling optical properties of porous silicon: Comparison with experiment," Phys. Status Solidi C 4, 1986–1990 (2007).
- <sup>19</sup>E. Xifré Pérez et al., Design, Fabrication and Characterization of Porous Silicon Multilayer Optical Devices (Universitat Rovira i Virgili, Tarragona, 2007).
- <sup>20</sup>H. H. Li, "Refractive index of silicon and germanium and its wavelength and temperature derivatives," J. Phys. Chem. Ref. Data **9**, 561 (1980).
- <sup>21</sup> J. M. Khoshman and M. E. Kordesch, "Optical properties of a-HfO<sub>2</sub> thin films," Surf. Coat. Technol. **201**(6), 3530–3535 (2006).
- $^{22}$  T. J. Bright, J. I. Watjen, Z. M. Zhang, C. Muratore, and A. A. Voevodin, "Optical properties of HfO<sub>2</sub> thin films deposited by magnetron sputtering: From the visible to the far-infrared," Thin Solid Films **520**, 6793–6802 (2012).
- <sup>23</sup> M. A. Green and M. J. Keevers, "Optical properties of intrinsic silicon at 300 K," Prog. Photovoltaics 3, 189–192 (1995).
- <sup>24</sup> J. Lee *et al.*, "Investigation of phonon coherence and backscattering using silicon nanomeshes," Nat. Commun. **8**(1), 14054 (2017).
- <sup>25</sup> M. H. Weik, "Fresnel reflection," in *Computer Science and Communications Dictionary*, edited by M. H. Weik (Springer, Boston, MA, 2001), p. 657.
- <sup>26</sup>J.-Q. Xi *et al.*, "Optical thin-film materials with low refractive index for broadband elimination of Fresnel reflection," Nat. Photonics 1(3), 176–179 (2007).
- $^{\bf 27}$  M. Michael, "On 'Aesthetic Publics': The case of VANTAblack "," (2018), https://journals.sagepub.com/doi/abs/10.1177/0162243918775217; accessed December 17, 2020.
- <sup>28</sup> A. Lundgren, "Vantablack—The closest thing on earth to nothing," (2014), accessed December 17, 2020. Available at: https://gupea.ub.gu.se/handle/2077/38112.
- <sup>29</sup> K. Colby, "The bind," Chic. Rev. **63**(3–4), 57 (2020).
- <sup>30</sup> A. Takakura *et al.*, "Strength of carbon nanotubes depends on their chemical structures," Nat. Commun. **10**(1), 3040 (2019).
- <sup>31</sup>D. Ogawa *et al.*, "Observation and characterization of fragile organometallic molecules encapsulated in single-wall carbon nanotubes," J. Nanomater. **2014**, 1, https://hindawi.com/journals/jnm/2014/539295/?cfid=749811706 & cftoken=73514595.xml; accessed December 17, 2020.
- 32 Method of manufacturing carbon nanotubes, https://technology.nasa.gov/public\_domain/GSC-14435-1; accessed December 17, 2020.
- <sup>33</sup>R. Rao *et al.*, "Carbon nanotubes and related nanomaterials: Critical advances and challenges for synthesis toward mainstream commercial applications," ACS Nano 12(12), 11756–11784 (2018).
- <sup>34</sup>M. Shao, D. D. D. Ma, and S. T. Lee, "Silicon nanowires—Synthesis, properties, and applications," Eur. J. Inorg. Chem. 2010(27), 4264–4278.
- <sup>35</sup>Z. H. Chen, J. S. Jie, L. B. Luo, H. Wang, C. S. Lee, and S. T. Lee, "Applications of silicon nanowires functionalized with palladium nanoparticles in hydrogen sensors," Nanotechnology **18**(34), 345502 (2007).